Channel Characterization of Magnetic Human Body Communication

Erda Wen, Daniel F. Sievenpiper, *Fellow, IEEE*, and Patrick P. Mercier, *Senior Member, IEEE*

***Abstract*— *Objective:* The objective of this paper is to model and experimentally validate the path loss benefits of magnetic human body communication (mHBC) using small form-factor-accurate coils operating under realistic conditions. *Methods:* A radiating near-field coupling model and numerical simulations are presented to show that the magnetic-dominant near-field coupling between resonant coils offers low path loss across the body and exhibits extra robustness to antenna misalignment compared to far-field RF schemes. To overcome the pitfalls in conventional vector-network-analyzer-based measurement configurations, we propose a standardized setup applied to broadband channel loss measurement with portable instruments. Two types of PCB coils for mHBC communication, designed for large devices such as smartphones and small devices such as earbuds, respectively, are built and measured. *Results*: The mHBC link for the ear-to-ear non-line-of-sight (NLOS) path measures up to -23.1 dB and -31.2dB with large and small coils, respectively, which is 50 dB more efficient than the conventional Bluetooth channels utilizing antennas of similar sizes. Ear-to-pocket and pocket-to-pocket channels also show at least 16 dB higher transmission than the Bluetooth channel. *Conclusion:* In terms of path loss, the mHBC approach offers compelling performance for short-range applications over the body region. For coils with dimensions of several centimeters, working between 100 MHz and 200 MHz minimizes the channel loss while keeping the bandwidth above 1 MHz. *Significance:* The extremely high efficiency of the proposed mHBC channel provides a solution to the energy problem for miniaturized wearables, potentially leading to new wearable device designs.**

***Index Terms*— Body area networks (BANs), human body communication (HBC), ultra-low power communication**

I. Introduction

THE rapid growth of wearable devices ranging from consumer electronics such as smartwatches and wireless headphones, to wearable medical sensors capable of recording parameters such as biopotentials [1], vital signs [2], physiochemistry [3], and more, are helping change personal lifestyles and the practice of medicine. Such devices require a wireless connection, established via a body area network (BAN), to communicate sensed data or interact with other electronic devices. However, commonly used far-field radio frequency (RF) techniques working at sub-6-GHz are extremely inefficient due to the large loss and reflection of the energy flux on the body surface [4], as illustrated in Fig. 1 (a). For miniaturized devices adopting these protocols, the radio system takes a large proportion of their power consumption, ultimately becoming the bottleneck of the achievable battery life [5]. As an example, in a typical EEG system, the Bluetooth Low Energy (BLE) Tx and Rx consume more than 70% of the power [6] [7]. For this reason, various forms of human body communication (HBC) approaches have been proposed to attempt to reduce path loss across the body. Examples include galvanic or capacitive HBC [8] [9] and near-field magnetic induction (NFMI) [11], and will be discussed in more detail in section II.

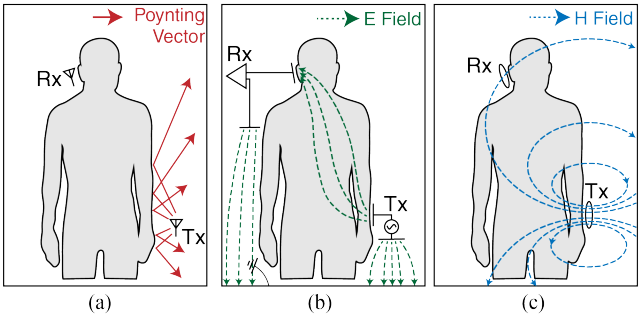

Fig. 1. Illustration of several common BAN approaches: (a) Far-field radio such as Bluetooth low energy (BLE); (b) capacitive HBC and (c) magnetic HBC

In this work, we model, analyze, and measure a radiative magnetic human body communication (mHBC) channel, targeting at low channel loss even under non-line-of-sight (NLOS) conditions across the human body. mHBC was first proposed in [12] for communication between a fixed access point and a wearable device and in [13] for communication between wearable devices, and has been shown experimentally with low-power integrated circuit-based implementations in [14]. However, recent studies on path loss modeling of the mHBC channel were based on quasi-static coupling [15], where the valid frequency and range are greatly limited. In this paper, Section III presents a the radiating near-field coupling model that provides analytical reasoning on why mHBC has advantages in both path loss and robustness. Also, due to the improper grounding of the experiment setup, the channel loss results in previous mHBC studies [14] [13] were overly optimistic, and for this reason, section IV and V presents a more rigorous measurement setup yielding more accurate results, while still validating the path loss advantages of mHBC under certain conditions.

The authors are with the University of California at San Diego, San Diego, CA 92093 USA (e-mail: ewen@ucsd.edu; dsievenpiper@ucsd.edu; pmercier@ucsd.edu).

II. Wireless Body Area Network Approaches

Similar to the categorization of wireless power transfer (WPT) schemes in [16], BAN approaches can also be categorized into several types in terms of frequency band and field component being used, as shown in Fig. 2. The traditional and widely-used approaches in the industry such as BLE, which works at 2.4 GHz, fall into the category of far-field transmission, since in most cases, both transmitting antenna and receiving antenna are placed in the far-field region of each other. The RF power transfers through propagating EM waves, following the classical Friis transmission equation in the free space. However, since the conductivity of human tissues is high at this high frequency, the signal suffers from a considerable shadowing effect across the body and presents large channel loss.

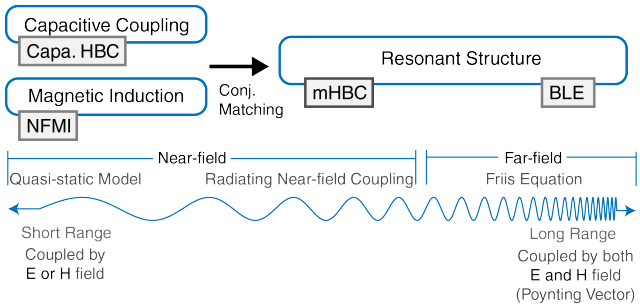

Fig. 2. Relationships between various BAN schemes and the corresponding modeling methods.

To address the body shadowing effect, recent studies have focused on systems working at significantly lower frequencies: for example into the sub-MHz regime, where the human body potentially performs as a conduit rather than a blockage. Assuming the field to be quasi-static, the signal is transferred primarily either through electric flux or magnetic flux. Unlike in far-field transmission, where the antennas need to be matched to the environment to create resonance at a certain frequency, in quasi-static cases, the environment itself is modeled as lumped elements being a part of a static circuit model. The fact that resonance is no longer necessary saves the effort to build conjugate matching networks and theoretically allows a wide bandwidth at the given (low) carrier frequency. On the other hand, the absence of resonance also makes the system inefficient.

Unlike these two schemes, the mHBC channel discussed in this work lies in between, taking advantage of both low losses of the human body at lower frequencies together with the high efficiency of resonant coupling. Neither the classical far-field transmission model nor the static circuit model is appropriate to characterize the coupling; instead, a radiating near field coupling model will be introduced in section III.

A. Far-Field RF (e.g., 2.4 GHz Bluetooth)

Although the BLE standard was initially designed for long-distance communication in free space, it has recently exploded in popularity for use in wearable devices such as smartwatches or wireless earbuds. Early studies of 2.4 GHz band channel loss across the human body showed promising results, when large antennas are being used with large spacing (over 6 cm) between the antenna and skin [17]. However, later studies show that a significant shadowing effect can be observed for more realistic cases involving non-line-of-sight (NLOS) paths with small antennas and shorter antenna-skin spacing (5 mm). For example, The difference between LOS and NLOS cases is over 20 dB for a 30-cm-long channel over the torso [18] [19]. A study on wireless hearing devices further estimates over 40 dB of attenuation due to the presence of the head for a 16 cm ear-to-ear channel, bringing the channel loss to 98 dB [4], which is incredibly large and requires significant energy-expensive signal amplification to close a link budget. This is one of the main reasons why BLE-based designs consume significant power in BANs.

B. Electro-quasistatic (EQS) Capacitive HBC

On the other side of the spectrum in Fig. 2, capacitive HBC was first proposed in 1996, suggesting communication through quasi-static electric fields at low frequencies [9]. Tx and Rx electrodes pairs are placed in close proximity to the skin to induce and detect the electric field around the body, respectively. The environment, including the body, can be modeled as RC circuits, and the path loss can then be estimated [10].

Much research has since been carried out with various terminating scenarios at various frequency bands up to several hundreds of MHz [20]- [26]. However, these early studies report a large variance in path loss, among which the most optimistic ones claim 20 dB loss across the body. Such low path loss was later shown to be not realistic, due to improper measurement configurations with poor ground isolation of large measurement equipment, which unintentionally creates an extra return path in the circuit model [27]. As demonstrated in [27], the best way to make accurate and realistic measurements is by utilizing small, form-factor-accurate wireless prototypes.

More recent studies adopt broadband high impedance termination, and report 40 dB LOS channel loss for 10 cm path with a 6 dB/10 cm decay rate, and a stable loss of 60 dB to 70 dB for very long-range NLOS channel over the whole body [15] [28]. Although the path loss turns out to be less appealing than what was initially expected, the capacitive HBC approach still outperforms conventional far-field RF approaches in efficiency especially for long NLOS channels, and has other advantages such as better privacy against eavesdropping [29] and less effort needed in engineering matching networks. However, more studies are needed to model and deal with the potentially high variability of the capacitive path during subject motion and environmental variation, which may add complexity to the circuit design for robust operation, particularly if inductors, which are difficult to tune, are used to resonate with the capacitive channel. For these reasons, capacitive HBC remains an area of active research and development.

C. NFMI

Similar to capacitive HBC, magnetic-induction-based near-field communication (NFMI) also proposes to use the non-

radiating field, but with a quasi-static magnetic field induced by coils rather than an electric field. To date, a widely accepted link budget model for this technique is not yet available [4]. Existing research on Tx and Rx systems focus on very short-range applications within 7 cm [30] [31]. A study on inductive MIMO design reports 30 dB attenuation for 20 cm separation in free space with multiple 20-cm-diameter coils [32]. Another survey on the mutual coupling between resonant coils wrapped on ferrite rods working in the NFC band (13.56 MHz) measured around a -100 dB coupling coefficient for a 15 cm path [33].

D. Magnetic HBC

Magnetic HBC was originally envisioned to exploit inductive resonant coupling between coils in the near-field to mid-field region for greater efficiency over a far-field radio. The initial intuition was based on the fact that the relative permeability of the body is close to that of air, and as a result the body should cause minimum interference with magnetic-dominant near-fields created by coils [13]. Based on this, an extremely power efficient transceiver prototype with Sub-10-pJ/bit 5-Mb/s was developed with OOK modulation [14] [34]. However, the coils adopted in the previous studies were large and wrapped around the limbs or forehead, which is not practical for form-factor-accurate wearable prototypes. In addition, the VNA-based mHBC channel loss measurement generates overly optimistic results in a similar manner to that in earlier eHBC papers, as described in [27]. As a result, this paper considers more realistic form factors and shows that small PCB coils, measured with an setup that minimizes any extra transmission path, still shows high efficiency and robustness to channel variations.

III. Characterization of Near-field mHBC Coupling

An electrically small current loop, with circumference much smaller than the wavelength ($C < \lambda/10$) can be regarded as a small magnetic dipole, whose moment is given by $I_m l = jS\omega\mu I_0$, in which S is the area of the loop. When placed along the z-axis, the fields generated can be described by

$$E_r = E_\theta = H_\phi = 0, \tag{1}$$

$$E_\phi = -jE_0 \sin\theta \left[\frac{1}{r} + \frac{1}{jkr^2}\right] e^{-jkr}, \tag{2}$$

$$H_r = 2H_0 \cos\theta \left[\frac{1}{kr^2} + \frac{1}{jk^2r^3}\right] e^{-jkr}, \tag{3}$$

$$H_\theta = jH_0 \sin\theta \left[\frac{1}{r} + \frac{1}{jkr^2} - \frac{1}{k^2r^3}\right] e^{-jkr}, \tag{4}$$

where $E_0 = kI_m l/4\pi$ and $H_0 = kI_m l/4\pi\eta$, with η being the characteristic impedance of free space. For long electrical distances $r \gg \lambda$, only the components with the term $1/r$ in H_θ and E_ϕ survive, forming a real Poynting vector in the $\hat{\mathbf{r}}$ direction, and that allows us to model the transmission by a simple Friis equation. However, at shorter distances, particularly when $r < \lambda/2\pi$, the $(1/kr)^2$ term is dominant, complicating the coupling coefficient calculation. In this section, we demonstrate with a radiating near-field coupling model that these near field components actually help improve the path loss performance as well as increase the robustness to antenna misalignment.

A. Formulation for Free-space Transmission

Consider a general case where a pair of transmitting antenna Tx and receiving antenna Rx are placed at a distance d in free space depicted in Fig. 3. The far-field transmission behavior between them can be described with Friis equation given the gain of each antenna, but for near-field scenarios, the energy couples through the whole space in between, rather than in a single direction, as a result, there is not a simple gain term that can be separated from the path loss component. Rather, we can treat the whole system consisting of both antennas and the region in between as a two-port network, the coupling coefficient S_{21} is by definition b_R/a_T, which is usually referred to as "coupling quotient" when power is the parameter of interest. Therefore, the transmission can be expressed by $|b_R/a_T|^2$ - the power coupled to the Rx antenna per unit of power incident to the transmitting antenna. This coupling quotient between the two antennas can be related to the vector far-field pattern of Tx and Rx antenna $\mathbf{f_T}(\mathbf{k})$ and $\mathbf{f_R}(-\mathbf{k})$ by [35]

$$\frac{b_R}{a_T} = -\frac{C_R}{k} \iint_{k_x^2+k_y^2<k^2} \frac{\mathbf{f_T}(\mathbf{k}) \cdot \mathbf{f_R}(-\mathbf{k})}{k_z} e^{j\mathbf{k}\cdot\mathbf{r}} dk_x dk_y, \tag{5}$$

where the wave number $\mathbf{k} = \hat{\mathbf{x}}k_x + \hat{\mathbf{y}}k_y + \hat{\mathbf{z}}k_z$ with the magnitude $k = 2\pi/\lambda$. C_R is the "mismatch factor" defined by

$$C_R = \frac{Z_f}{\eta(1 - \Gamma_L\Gamma_0)}, \tag{6}$$

in which Γ_L and Γ_0 are the reflection coefficients of the receiving antenna and its passive termination, respectively. Z_f is the characteristic impedance of the output port. In the following analysis, we assume all ports are perfectly matched with no reflections, i.e., $\Gamma_L = \Gamma_0 = 0$.

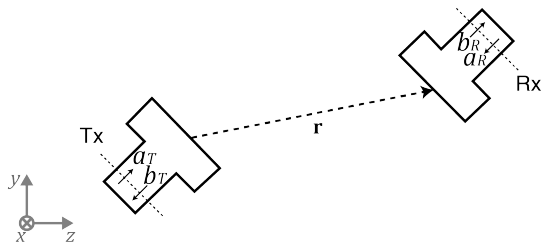

Fig. 3. Antenna placement for near-field coupling modeling.

For the far-field case where $kr \gg 1$, it can be shown that (5) is reduced to the Friis transmission equation

$$\left|\frac{b_R}{a_T}\right|^2 = |\mathbf{f_T}(\mathbf{r}) \cdot \mathbf{f_R}(-\mathbf{r})|^2 \frac{\lambda^2}{(4\pi r)^2}. \tag{7}$$

This equation indicates that more power is lost at higher frequencies, assuming the antenna pattern remains isotropic,

This article has been accepted for publication in a future issue of this journal, but has not been fully edited. Content may change prior to final publication. Citation information: DOI 10.1109/TBME.2021.3101766, IEEE Transactions on Biomedical Engineering

which is usually the case for a miniaturized antenna; thus lower frequencies are preferred. This conclusion can also be drawn by considering the effective length of a resonant dipole along the z-axis:

$$l_{\text{eff}} = \frac{\lambda}{\pi}\frac{cos(\pi/2\cos\theta)}{\sin\theta} \tag{8}$$

By comparing (5) and (7), it can be seen that unlike the far-field transmission, where the coupling depends on the gain in a single direction connecting Tx and Rx, the coupling coefficient in the near-field region is an integral of the pattern in all directions. This helps to eliminate the effects of pattern nulls in certain directions [36].

Note that in (5), a singularity occurs when $k_x^2 + k_y^2$ approaches k^2. One way to avoid this is to express it in a series form [35] [37]

$$\frac{b_R}{a_T} = \sum_{n=0}^{\infty} B_n h_n^{(1)}(kd), \tag{9}$$

$$\begin{aligned} B_n = &- C_R \frac{2n+1}{2} j^n \\ &\times \int_0^{\pi}\int_0^{2\pi} \mathbf{f_T}\cdot\mathbf{f_R} P_n^0(\cos\theta_0)\sin\theta_0 d\phi_0 d\theta_0, \end{aligned} \tag{10}$$

where $h_n^{(1)}$ represents the spherical Hankel functions of the first kind and $P_n^0(\cos\theta_0)$ is the associated Legendre polynomials. This equation also assumes that both antennas are placed on the z-axis separated at a distance of d. The doughnut-shaped pattern of a horizontally placed current loop is described as

$$\mathbf{f}(\theta,\phi) = \hat{\theta}\sqrt{3/2}\sin\theta. \tag{11}$$

Fig. 4 shows the results of the transmission $|b_R/a_T|^2$ with respect to distance for various kinds of dipole placement, by applying (11) to (9) and (10). The results of FEM numerical simulation in Ansys HFSS are also plotted for comparison with two perfectly matched 5cm-diameter coils working at 200 MHz. Each coil is placed either horizontally, vertically, or at 45 degrees. Note that the far-field pattern has a null that occurs along the z-direction for a horizontally placed loop. Yet, in the near-field region, the coupling along this direction still exists and is even larger than that in the broadside direction for a short-range when $d < 0.5m$. This provides near-field communication with extra robustness in terms of antenna orientation.

It is worth noting that since the radiative parts of the field components are being used, it has less advantage in anti-eavesdropping or anti-jamming compared to quasi-static models. Nevertheless, the lower channel loss of the system compared to conventional far-field radios may allow a lower transmitting power, and as a result makes it less easy to eavesdrop.

B. Body Effect

The effect of the human body on radiation, when located close to an antenna, is complicated. Besides simple reflection, refraction, and near-field dielectric and ohmic loss, other mechanisms also exist, such as surface waves [23] or lossy

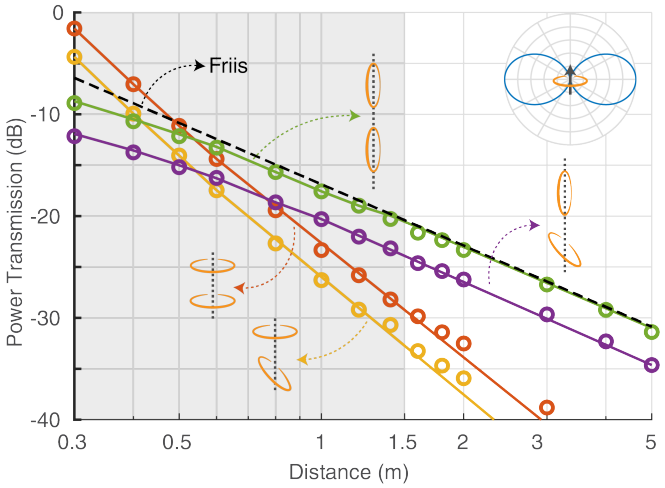

Fig. 4. Coupling between two small loops representing magnetic dipoles, working at 200 MHz. Solid line: theoretical calculation with the near-field coupling model; circles: FEM simulation results.The shadowed area represents near field region where the separation $d < \lambda$.

waveguide effects. Analytical models have been put forward on simple cases such as a small dipole surrounded by lossy dielectric [38] or near a reflective half-space [39] to demonstrate that the near-field magnetic antennas hold superiority over electric antennas with regard to near-field loss and penetration. A brief explanation is that the dissipation inside the tissue can be expressed as $L = \int \sigma \mathbf{E}\mathbf{E}^* dV$ without involving magnetic components; thus, transmission through magnetic fields is preferable.

Fig. 5 provides the dielectric properties of various human body tissue from 10 MHz to 10 GHz based on [42]. Conductivity sees a rapid increase above 1 GHz, reaching around 2 S/m for muscle in the 2.4 GHz BLE band. This makes the body appear as a conductor, and the reflection is therefore quite severe. Besides this, since body parts are electrically large compared to the wavelength (12.5 cm), diffraction is weak, explaining the huge shadowing for the NLOS path. Similarly, the high relative permittivity, especially below 100 MHz, explains the extensive path loss in the electric field dominated HBC channel.

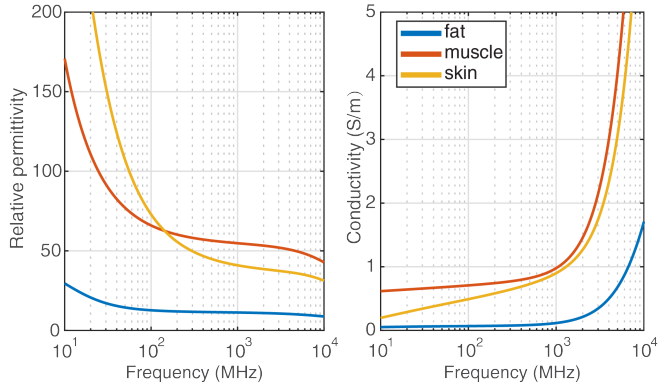

Fig. 5. Dielectric properties of human body tissue with respect to frequency.

Given the complexity of the interaction between the antenna

and the body tissue, numerical solutions are generally involved to evaluate the performance under particular circumstances [40] [41]. To better illustrate the lower loss and stronger diffraction at lower frequencies, Fig.6 shows FEM simulation results of the magnetic field induced by a small magnetic dipole close to a 16-cm-wide 3D head model. The dielectric properties are set to be the frequency-dependent average of human tissue over the body weighted by their relative volumes, and the dipole is placed close to the ear, 3mm away from the skin. Fig. S1 in the supplementary materials shows that at the frequency of interest, the results with average electric property of the tissue is close enough to that with a multi-layered model. The results validate the increasing loss when the frequency rises. Note that at 200 MHz, the magnetic field penetrates the dielectric region easily, whereas at 2.4 GHz, the skin depth becomes so small that the power hardly reaches the other side of the head. The difference between them is as high as around 45 dB, which is consistent with the extra loss brought by head blockage for BLE signals estimated in [4].

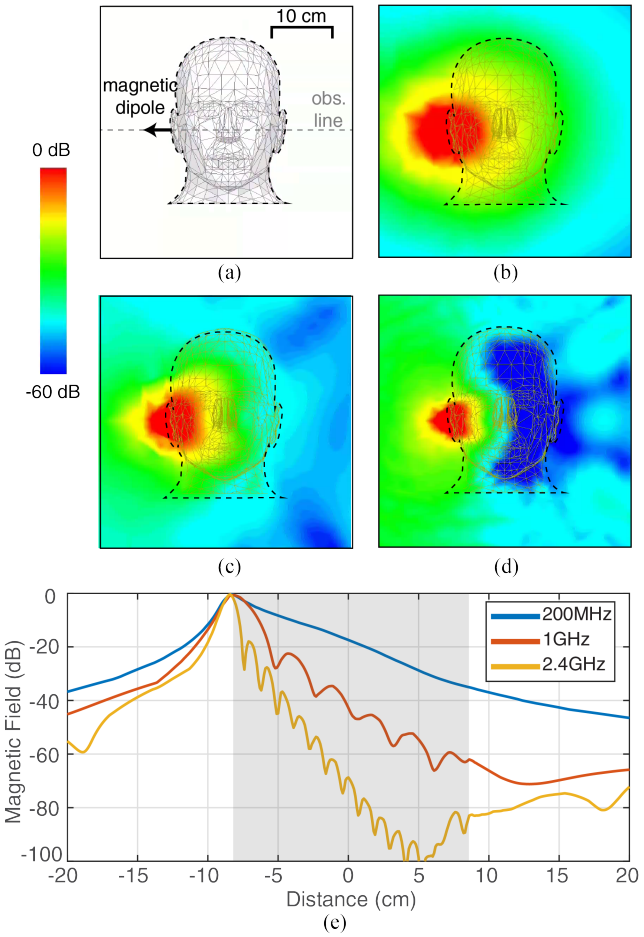

Fig. 6. Simulation results of a magnetic dipole close to a 3-D head model. (a) The geometry of the simulation setup; (b), (c) and (d) are the induced magnetic field intensity at 200 MHz ,1 GHz and 2.4 GHz, respectively; (e) field intensity plot along the observation line, normalized to maximum value, the shadowed area represents the dielectric head region.

IV. Measurement Configuration Comparisons

Our group's previous research provided evidence that the poor ground isolation for various measurement platforms is to blame for the vast discrepancy in measured channel loss among earlier studies in capacitive HBC [27]. First of all, methods involving a common ground for Tx and Rx are essentially not qualified as "wireless communication" because their grounds are connected with "wires", creating a direct return path between Tx and Rx. Even in the cases where instruments are separately grounded, other capacitive return paths still exist between the large ground planes over large equipment such as a vector network analyzer (VNA), signal generator (SG), spectrum analyzer (SA), or oscilloscope. Under these circumstances, the path loss is significantly underestimated. Measures like introducing Balun structures can help, but the improvement is limited. The most accurate way to measure path loss in a capacitive HBC system is by using a carefully designed, form-factor-accurate battery-operated prototype. This work will show that similar pitfalls exist for mHBC measurement operating with radiative content; this is the main reason why prior mHBC measurements were overly optimistic. To address this, we here propose a convenient, standardized platform with portable RF equipment for broadband channel loss measurement.

A. VNA-based Measurements

Conventional VNA-based measurements characterize path loss by equivalently evaluating the maximum available gain (MAG) between the devices under test (DUTs):

$$\mathrm{MAG} = \frac{|S_{21}|}{|S_{12}|} \times \left(K - \sqrt{K^2 - 1}\right), \tag{12}$$

$$\text{where } K = \frac{1 - |S_{11}|^2 - |S_{22}|^2 + |\Delta|^2}{2\,|S_{12}S_{21}|}, \tag{13}$$

$$\text{and } \Delta = S_{11}S_{22} - S_{12}S_{21}. \tag{14}$$

For a reciprocal system, this can be reduced to a simpler form:

$$\mathrm{MAG} = \frac{|S_{21}|^2}{\left(1 - |S_{11}|^2\right)\left(1 - |S_{22}|^2\right)}, \tag{15}$$

which has a more explicit physical meaning that the path loss is the power transfer between the antennas, after deducting the power reflected at both Tx and Rx ports due to mismatch. Assuming the Tx and Rx are perfectly matched, MAG will be further reduced to simply $|S_{21}|^2$. Compared to "path loss", MAG also takes into account the dissipation loss, including the conductive loss and the dielectric loss from the antenna itself, which makes it a more practical index. In other words, the transmission coefficient between the given Tx and Rx antenna can practically reach MAG by applying a lossless lumped or distributed matching network.

Such a VNA-based measurement works fine for unbalanced DUTs with a stable ground plane, such as monopoles or patch antennas. However, when it comes to balanced structures such as coils, dipoles, or a pair of electrodes, the current can flow directly back on the outer conductor of the coaxial cable.

The cable can be consequently considered part of the antenna and changes the transmitting characteristics completely, as illustrated in Fig. 7. This effect worsens when the antennas are relatively smaller than the long cables, since more transmission power goes through the coax and overwhelms the coupling between Tx and Rx directly.

Several strategies can be used to address this issue. A Balun structure isolates the antenna from the ground of the coaxial cables: for narrow-band applications, one may use structures like choking sleeve [44]; for broadband cases, one may use a Balun transformer. Unfortunately, the parasitic interwinding capacitance over the transformer still provides an indirect path for RF signals, and the unbalanced current can not be entirely eliminated. Another approach is to apply RF sheet absorbers around the cable to dampen its radiation.

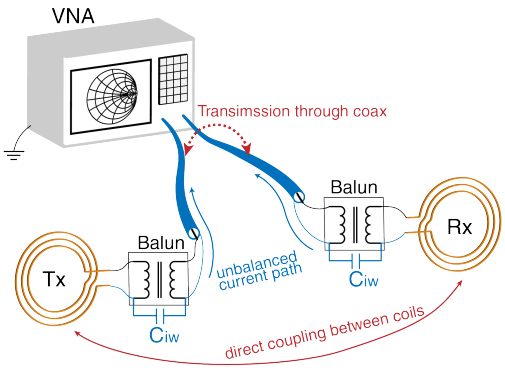

Fig. 7. Illustration of why the conventional VNA-based measurement suffers from signal coupling between long cables.

B. Measurement with Portable SG and SA

A more straightforward way to reduce unwanted radiation is to adopt no cables and miniaturized equipment, such as a handheld signal generator and spectrum analyzer as in Fig. 8. However, the load of the RF SG needs to be tuned to 50Ω to obtain a valid measurement of the incident power. This can be achieved by inserting a matching network, but this is hard to realize over a broad frequency band. We propose an alternative solution: apply a resistive attenuator to stabilize both the load impedance for the SG and the antenna's source impedance. The impedance looking into one side of a 50Ω attenuator depends on the load on the other side, but is always close to 50Ω if the attenuation is large enough. For example, the impedance from one side of the 15 dB attenuator used in Fig. 8, at two extreme cases, is $72\Omega//136\Omega = 47.1\Omega$ for a short circuit load and $72\Omega//(136\Omega + 72\Omega) = 53.5\Omega$ for an open-circuit load. As a result, the signal generator sees a 50Ω load, and the antenna sees a 50Ω port so that (15) remains valid, as long as 15 dB is added to S_{21} to compensate the forward power loss on the attenuator:

$$S_{21}\ (\text{dB}) = P_{SA} - P_{SG} + 15\ (\text{dB}). \tag{16}$$

To compare the measurement configurations discussed above, Fig. 9 shows the measured MAG between two 8-cm-diameter 2-turn copper coils wrapped around the arm, with

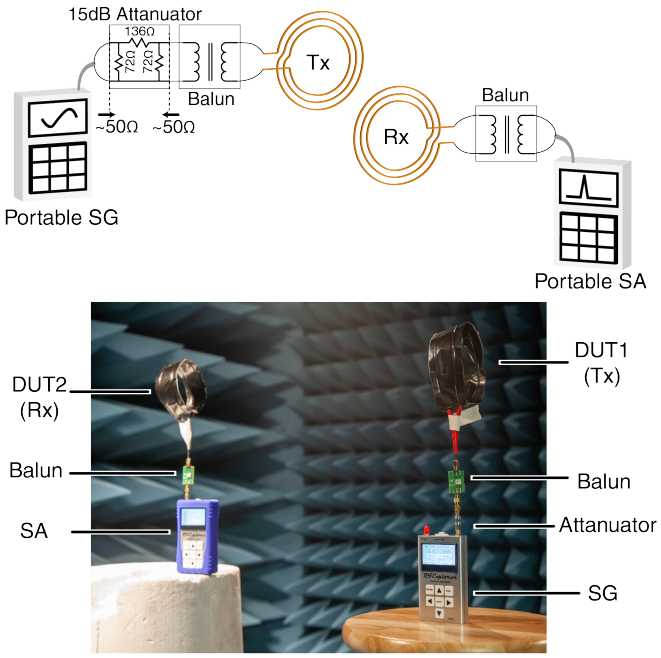

Fig. 8. The proposed measurement platform.

respect to different distances. The operating frequency is set to 21 MHz as in previous mHBC reports. The two cables used in VNA-based setups are 1.2 m and 1.8 m, respectively. We use MABA-011108 transformer from MACOM as the Balun chip, and double layers of 0.5 mm sub-microwave absorbing sheet MR5 by MAST Technologies as the absorber surrounding the coaxial cables.

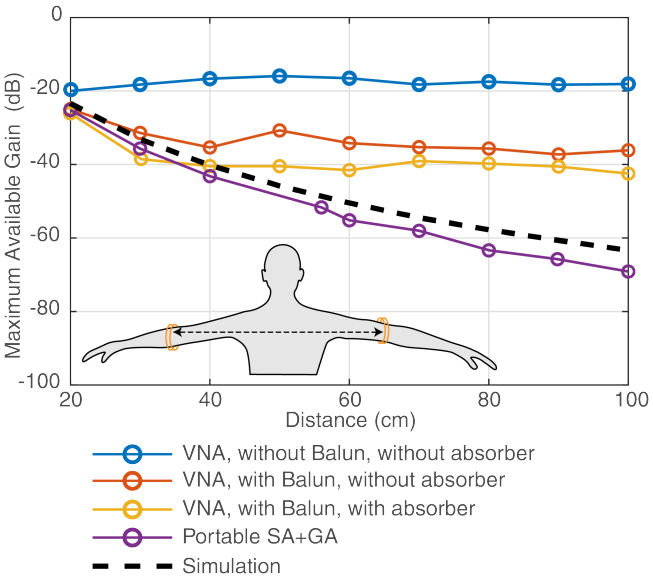

Fig. 9. Measurement results of different experimental setups with wrap-around coils on arms with different separations, compared to simulations.

The results with portable SG and SA matched exceptionally well with the simulation results, confirming the setup yields reliable and accurate results with minimum unwanted transmission, without applying any matching networks. The

absorber and the Balun only help for short separation where the transmission between Tx and Rx are dominant over the weakened radiation from the cables. This also confirms the argument in [28] that the inter-devices transmission is already too high at 20 MHz to keep the quasi-static model valid.

V. Results

We use two types of coils to examine the performance of the near-field mHBC, shown in Fig. 10: a) 4-turn PCB coils C1 with an outer diameter of 6 cm, which can fit into relatively large wireless devices such as smartphones or overhead headphones, and b) 4-turn PCB coils C2 with an outer diameter of 1.5 cm, designed for earbuds or other small wearables. For all measurements, C1 is placed parallel to, and 2 mm away from the skin separated by a foam, and C2 is directly plugged inside the auricle to emulate the working environment of an in-ear hearing device the orientation of which is the same with C1 For the BLE channel as a comparison, we use a Compact Reach Xtend Bluetooth antenna from Texas Instruments.

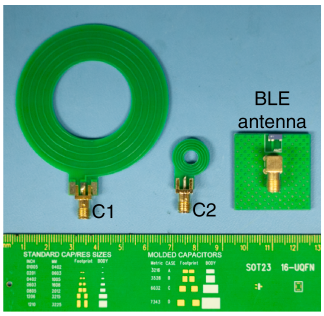

Fig. 10. PCB coils and Bluetooth antenna used in the measurements.

The channel loss for four scenarios are studied: a) a 16 cm ear-to-ear channel; b) a 30 cm pocket-to-pocket channel, where the antennas are put inside the cotton side pockets of jeans parallel to the skin; c) an 80 cm ear-to-pocket channel on the same side, and d) an 85 cm ear-to-pocket channel on the opposite side. The measurements are done over a 170-cm-tall male subject. RFE6GEN Combo and WSUB1G+ from RF Explorer are used as the signal generator and spectrum analyzer, respectively. The average value and standard deviation is calculated with four sets of independent measurements for each channel. The slight changes in antenna orientation due to body movements are allowed between each set as a verification on robustness.

As a baseline study, Fig. 11 shows the measured Bluetooth channel loss. Since the antenna is unbalanced and surrounded by the ground plane on the PCB, the VNA-based setup can be used without the unbalanced current issue. The results confirm the large shadowing effect in the NLOS path: ear-to-ear and pocket-to-pocket channel, where the path is blocked by the head and the thigh respectively, shows extremely high attenuation for a short path distance. The ear-to-pocket channel on the same side, on the other hand, shows less attenuation since the path is only blocked by the arm, which is relatively small and far away from the antennas. Nevertheless, the path loss for all four channels is above 65 dB, with a large deviation for NLOS cases due to fast fading.

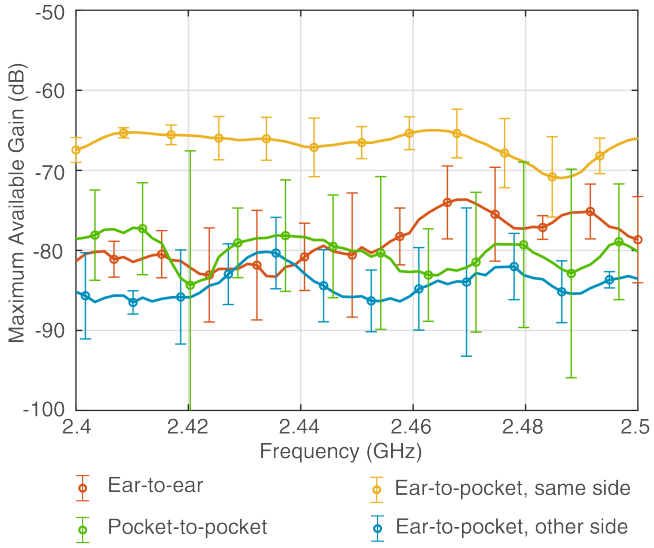

Fig. 11. Measured Bluetooth channel loss.

A. mHBC Coils Characteristics

Fig. 12 shows the input impedance of C1. This is as expected for a loop antenna, with the first resonance occurring around 185 MHz. To estimate the achievable resonant bandwidth of this loop working at different frequencies, we can examine its quality factor $Q \equiv 1/BW$ by the first-order estimation regarding the antenna impedance $Z = R + jX$ given in [43]:

$$Q \approx \omega \frac{|dZ/d\omega|}{2R} \tag{17}$$

It is worth noting that the bandwidth is beyond the Wheeler/Chu limit due to the presence of the human body as a lossy load on the antenna. Even so, for communication at lower frequencies, the bandwidth is still the main concern. As in this case, the bandwidth of C1 operating below 50MHz shrinks to under 1 MHz. For Rx systems, deliberately introducing loss using lumped resistors can broaden the bandwidth by compromising the available gain. As far as Tx is concerned, injection-locking can be used to effectively create a real-time match [14].

Similarly, Fig. 13 shows the input impedance and calculated bandwidth of C2. Being much smaller than C1, its quality factor is higher as expected. Thus, it faces bigger challenges in bandwidth operating at the low-frequency end.

B. mHBC Channel Loss

Fig. 14 shows the measured MAG of C1 serving as both the antenna over the ears and inside pockets. The measurement is carried out in a microwave anechoic chamber. For each scenario, four sets of data are collected. The output power of the SG is set to 10 dBm, and the results below the noise level are not plotted. The full-wave simulation results are also given for comparison over a 3D model of a 173-cm-tall male subject. While models with layered tissue are available, the complicated fine structures prohibitively consume too much

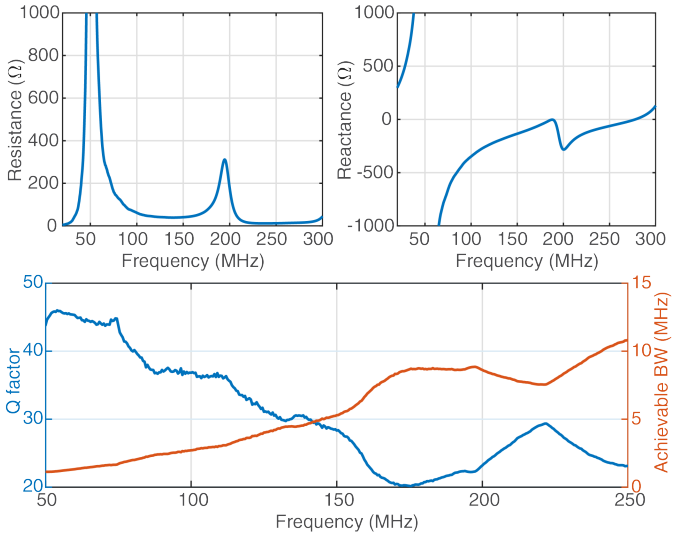

Fig. 12. Input impedance, calculated Q, and achievable bandwidth of C1.

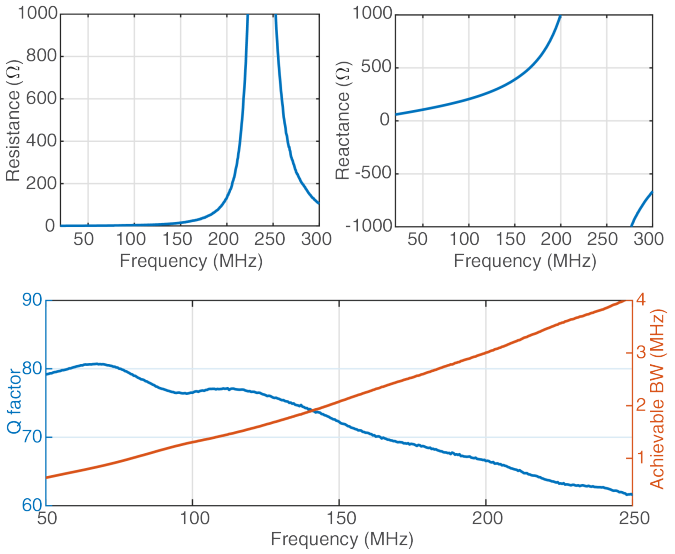

Fig. 13. Input impedance, calculated Q, and achievable bandwidth of C2.

computing resources. Thus frequency-dependent averaged dielectric properties are used instead. The measurement results show reasonable agreement with the simulation, whereas the channel loss for longer path even reveals slightly better performance than the simulation.

In the previous section, we discuss how lower frequencies win with better penetration and diffraction over body tissue. Yet, in both measurement and simulation, the maximum available gain starts to flatten and drop below frequencies of around 100 MHz to 150 MHz. To better illustrate what limits the transmission level at the lower frequency end, we conduct another set of simulations over the body with the same setup except having the copper material replaced by perfect electric conductor (PEC), as shown in Fig 16. Since the loss of the copper barely affects the radiating field distribution, the difference between the two cases represents the conductive loss from the coils themselves. Consequently, the radiation efficiency in terms of each channel can be estimated by

$$\eta = 10^{\frac{\mathrm{MAG_{copper}(dB)} - \mathrm{MAG_{PEC}(dB)}}{10}} \tag{18}$$

As far as the lossless case is concerned, the simulation indeed predicts that the path loss keeps improving as the frequency decreases. Still, as the reflection coefficient approaches 1 at frequencies below 100 MHz, where the antenna hardly radiates, the dissipation dominates the power consumption, resulting in a drastic drop in efficiency, canceling out the advantages in path loss. In conclusion, the miniaturized radiating near-field coil suffers a similar efficiency problem with a miniaturized far-field antenna.

As an example to prove that transmission can reach MAG by proper matching, Fig. 17 presents the measured S_{11} and S_{21} of the ear-to-ear channel: at the resonant frequency at around 185 MHz the transmission indeed approaches the MAG. Moreover, the transmission level surpasses that of Bluetooth in Fig.11 within the entire band shown in Fig. 17 even under large mismatch.

In addition to the independent measurements of a static posture that reflects the variation of the channel due to slight body movement, Fig.18 show the variation of channel loss between different body stances. Since the ear-to-ear channel usually suffers less misalignment between the antennas attached tightly to both ears, we investigate the impact of three types of motion on the ear-to-pocket (same side) channel: turning the head around 60 degrees towards left or right, or moving the pocket antenna from the side to the front of the thigh, as Fig.18 (a) illustrates. The coils are still placed parallel to the skin so the orientation changes with the motion accordingly. The mHBC channel experience significantly less variation than the far-field 2.4 GHz transmission against the body motion as expected.

Fig. 15 shows the MAG measurement results of replacing the over-ear C1 to in-ear C2 to examine the path loss with smaller antennas for miniaturized hearing devices. A larger path loss can be observed than that with C1 only, as the antenna is closer to the skin and surrounded by the ear tissue, experiencing more absorption. Nevertheless, the ear-to-ear channel still far surpasses BLE, and the pocket-to-ear channel also shows promising low loss around 180 MHz. Fig. 19 shows the radiation efficiency of the channels in this case. Since the coils have a much smaller electrical size, the simulation is taken more carefully to warrant the accuracy of the radiation to evaluate the efficiency. Finite Element-Boundary Integral (FEBI) boundary is used to reduce the impact of the boundary to the antenna, and a finite-conductive impedance sheet with $\sigma = 5.8 \times 10^7 S/m$ is used to represent the copper with finer meshing. As expected, with a smaller dimension of C2, the efficiency is even lower than the channel with C1, prohibiting the adoption of very low-frequency operation.

Table I summarizes the path loss of BLE, EQS capacitive HBC, NFMI, as well as mHBC in this work. Since few studies report on NFMI channel modeling and measurements, we conduct a FEM simulation with 25-turn copper coils wrapped around a 2.5-cm-long ferrite cylinder with a 4 mm diameter.

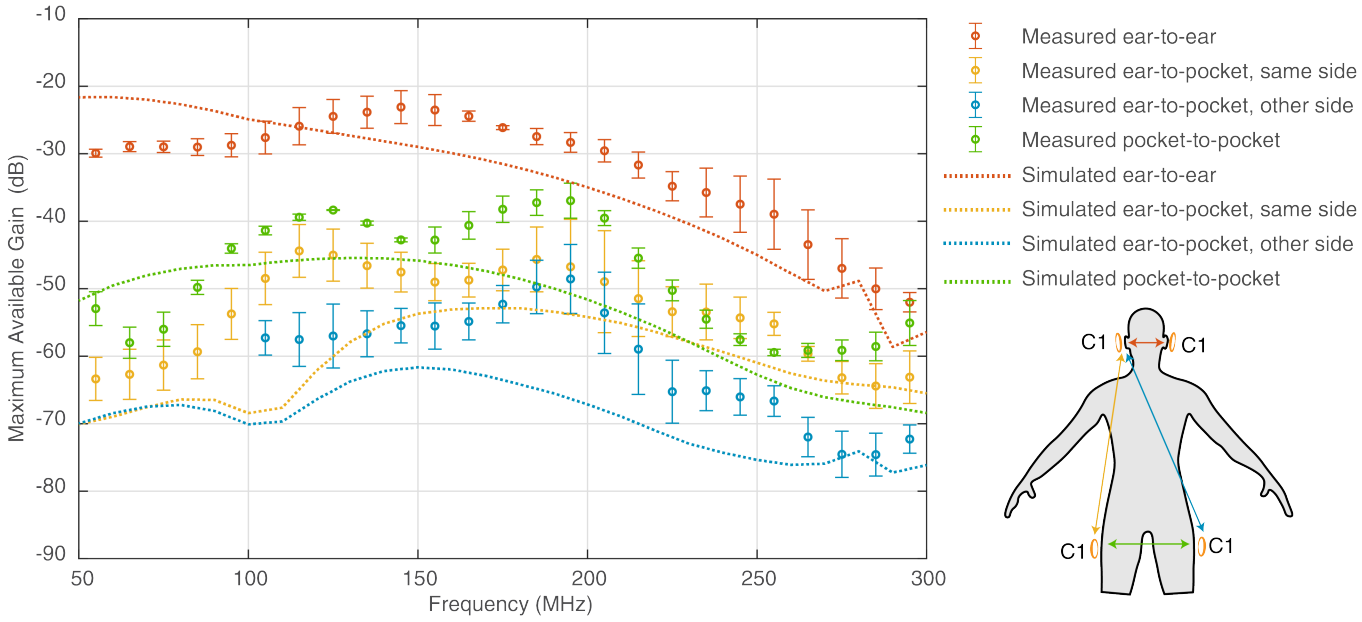

Fig. 14. MAG simulation and measurement results of various channels with C1 coils placed over the ear and/or inside pants pockets.

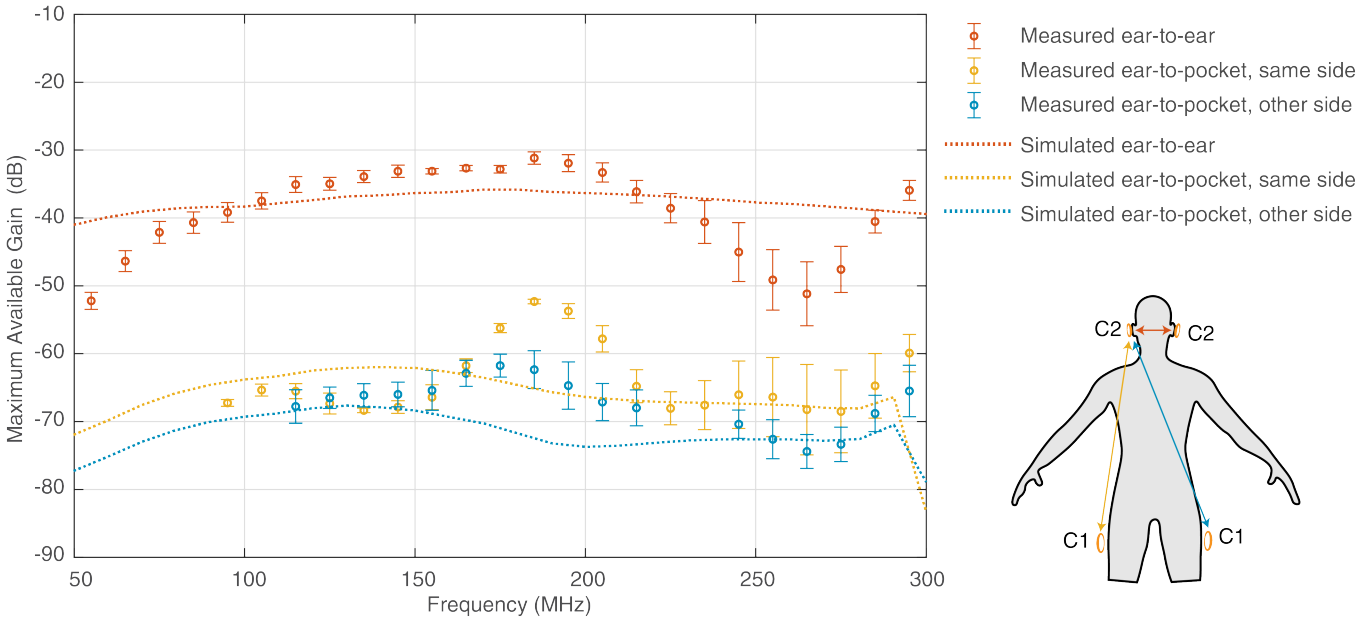

Fig. 15. MAG simulation and measurement results of various channels with C2 coils placed in the ear canal and/or C1 coils inside pants pockets.

TABLE I
COMPARISON OF PATH LOSS

Path Gain/MAG	Ear-to-ear	Ear-to-pocket (same side)	Ear-to-pocket (other side)	Pocket-to-pocket
mHBC, C1 (measured)	-23.1 dB @ 145 MHz	-46.7 dB @ 195 MHz	-48.6 dB @ 195 MHz	-37.0 dB @ 195 MHz
mHBC, C2 (measured)	-31.2 dB @ 185 MHz	-51.1 dB @ 185 MHz	-62.4 dB @ 185 MHz	N/A
BLE @ 2.4 GHz (measured)	-81.3 dB	-67.5 dB	-85.2 dB	-78.6 dB
EQS capacitive HBC @ below 20 MHz (reported in [28] [15], similar distances)	∼ -46 dB (LOS)	∼ -61 dB	∼ -61 dB	∼ -57 dB (LOS)
NFMI, resonant @ 13.56 MHz (simulated)	-51.3 dB	-84.0 dB	-85.0 dB	-58.3 dB
NFMI, resonant @ 13.56 MHz (reported in [33])	-109 dB to -103 dB	N/A	N/A	N/A

VI. CONCLUSION

This work demonstrates analytical modeling and the measurement results of resonant magnetic human body communication between PCB coils across the body. Magnetic

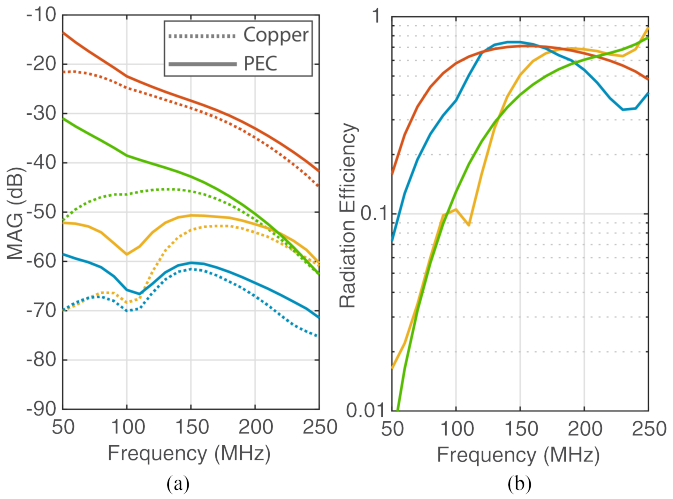

Fig. 16. Simulation results with different loss setups for C1 channels. (a) MAG comparison between copper coils and PEC coils. The color legends are the same as Fig.14; (b) Estimated radiation efficiency with the simulation results for each channel with C1 antenna.

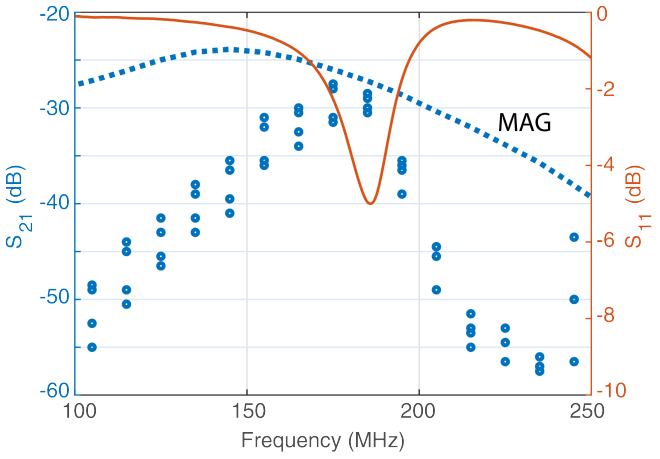

Fig. 17. S_{11} and S_{21} of ear-to-ear channel. Blue dots: S_{21} with (16), blue dotted curve: maximum available gain, and red curve: reflection coefficient.

dominant near-field communication shows advantages in path loss compared to other BAN approaches. However, several factors need to be considered in practical applications: on the one hand, lower frequencies are preferable since:

1) effective length of a resonant coil, performing like a magnetic dipole, increases for longer wavelength;
2) lower conductivity of body tissue reduces the specific absorption rate (SAR) and thus increases the efficiency, and
3) better diffraction can be achieved as the body becomes electrical smaller and therefore minimizes its shadowing effect.

On the other hand, several drawbacks exist when using very low frequencies:

1) the bandwidth drastically decreases, especially for small antennas, making it difficult to communicate with high throughput;
2) the dissipation loss inevitably decreases the efficiency at low frequencies where the coil barely radiates, and

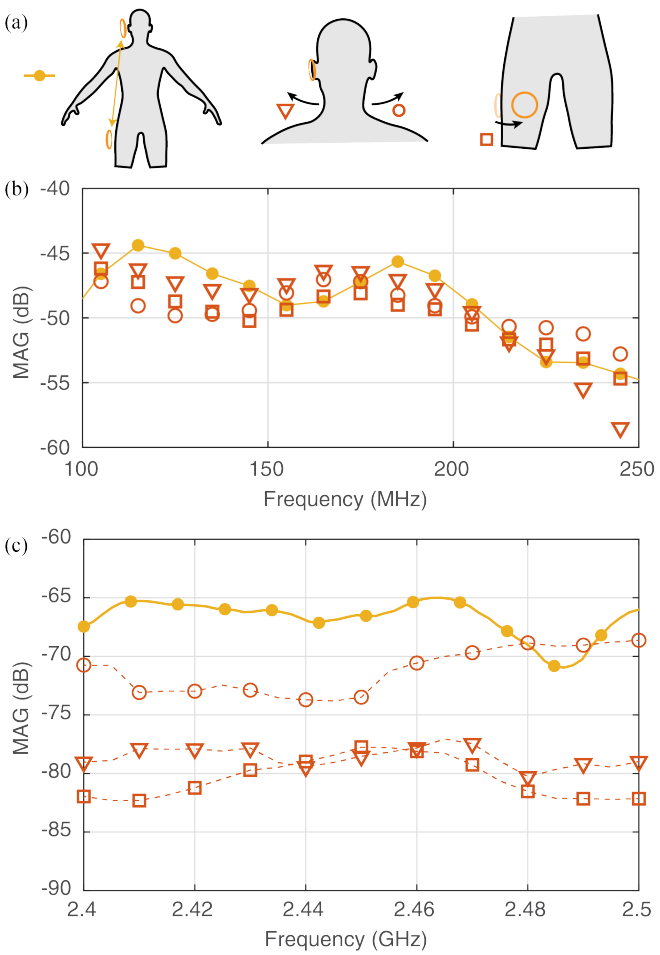

Fig. 18. Variation of the ear-to-pocket (same side) channel loss due to larger-scale body motions. (a) The illustration and the legend of different postures: original standing stance (yellow line), turning the head to the left (red circle), turning the head to the right (red triangle), and placing the coil to the front of the thigh (red square). (b) Measured mHBC channel with C1 coils. (c) Measured 2.4 GHz band with BLE antennas.

3) if lumped matching networks are to be avoided for efficiency considerations, miniaturized antenna geometry needs to be elaborately engineered and tuned as in [45] and [46]. The matching gets exponentially more challenging when the frequencies are extremely low.

Considering this trade-off, we find that for antennas with a dimension of several centimeters, the preferable operating frequency lies between 100 MHz to 200 MHz, where mHBC outperforms the conventional BLE channel by at least 40x under moderate body blockage (ear-to-pocket, same side), and up to 100,000x under high body blockage (ear-to-ear).

REFERENCES

[1] G. Acar et al, "Wearable and Flexible Textile Electrodes for Biopotential Signal Monitoring: A review," *Electronics-Switz*, vol. 8, no. 5, May 2019, doi: ARTN 479 10.3390/electronics8050479.
[2] Y. Khan et al, "Monitoring of Vital Signs with Flexible and Wearable Medical Devices," *Adv Mater*, vol. 28, no. 22, pp. 4373-4395, Jun 8 2016, doi: 10.1002/adma.201504366.
[3] S. Imani et al., "A wearable chemical-electrophysiological hybrid biosensing system for real-time health and fitness monitoring," *Nature Communications*, vol. 7, May 2016, doi: ARTN 11650 10.1038/ncomms11650.

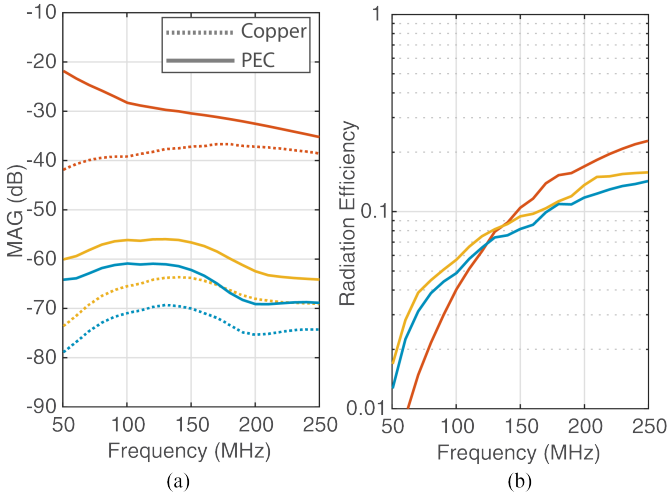

Fig. 19. Simulation results with different loss setups of channels using C1 and C2. (a) MAG comparison between copper coils and PEC coils. The color legends are the same with Fig.15; (b) Estimated radiation efficiency with the simulation results for each channel with C1 and C2 antenna.

[4] J.-C. Edelmann and T. Ussmueller, "Can you hear me now?: Challenges and benefits for connectivity of hearing aids and implants," *IEEE Microw Mag*, vol. 19, no. 7, pp. 30-42, 2018.

[5] P. P. Mercier and A. P. Chandrakasan, *Ultra-low-power Short-range Radios*. Springer, 2015.

[6] "2.4-GHz Bluetooth ® low energy System-on-Chip," in "*Technical Report October 2010*," Texas Instruments, 2013.

[7] "RHD2000 Series Digital Electrophysiology Interface Chips," Intan Technologies, 2012.

[8] M. S. Wegmueller et al, "Signal Transmission by Galvanic Coupling Through the Human Body," *IEEE T Instrum Meas*, vol. 59, no. 4, pp. 963-969, Apr 2010, doi: 10.1109/Tim.2009.2031449.

[9] T. G. Zimmerman, "Personal area networks: Near-field intrabody communication," *Ibm Syst J*, vol. 35, no. 3-4, pp. 609-617, 1996, doi: DOI 10.1147/sj.353.0609.

[10] S. Maity, M. X et al, "Bio-Physical Modeling, Characterization, and Optimization of Electro-Quasistatic Human Body Communication," *IEEE T Bio-Med Eng*, vol. 66, no. 6, pp. 1791-1802, Jun 2019, doi: 10.1109/Tbme.2018.2879462.

[11] A. Pal and K. Kant, "NFMI: Connectivity for Short-Range IoT Applications," *Computer*, vol. 52, no. 2, pp. 63-67, Feb 2019, doi: 10.1109/Mc.2019.2892862.

[12] T. Ogasawara et al, "Human Body Communication Based on Magnetic Coupling," *IEEE Transactions on Antennas and Propagation*, vol. 62, no. 2, pp. 804-813, Feb 2014, doi: 10.1109/Tap.2013.2292705.

[13] J. Park and P. P. Mercier, "Magnetic Human Body Communication," *IEEE Eng Med Bio*, pp. 1841-1844, 2015. [Online]. Available: Go to ISI://WOS:000371717202033.

[14] J. Park and P. P. Mercier, "A Sub-10-pJ/bit 5-Mb/s Magnetic Human Body Communication Transceiver," *IEEE J Solid-St Circ*, vol. 54, no. 11, pp. 3031-3042, Nov 2019, doi: 10.1109/Jssc.2019.2935549.

[15] M. Nath et al, "Understanding The Role of Magnetic and Magneto-Quasistatic Fields in Human Body Communication," *arXiv preprint arXiv:2011.00125*, 2020.

[16] H. J. Kim et al, "Review of Near-Field Wireless Power and Communication for Biomedical Applications," *IEEE Access*, vol. 5, pp. 21264-21285, 2017, doi: 10.1109/Access.2017.2757267.

[17] P. S. Hall et al., "Antennas and propagation for on-body communication systems," *IEEE Antenn Propag M*, vol. 49, no. 3, pp. 41-58, Jun 2007, doi: 10.1109/Map.2007.4293935.

[18] A. Fort et al, "Ultra-wideband channel model for communication around the human body," *IEEE J Sel Area Comm*, vol. 24, no. 4, pp. 927-933, Apr 2006, doi: 10.1109/Jsac.2005.863885.

[19] E. Reusens et al., "Characterization of On-Body Communication Channel and Energy Efficient Topology Design for Wireless Body Area Networks," *IEEE T Inf Technol B*, vol. 13, no. 6, pp. 933-945, Nov 2009, doi: 10.1109/Titb.2009.2033054.

[20] N. Cho et al, "The human body characteristics as a signal transmission medium for intrabody communication," *IEEE T Microw Theory*, vol. 55, no. 5, pp. 1080-1086, May 2007, doi: 10.1109/Tmtt.2007.895640.

[21] R. Y. Xu et al, "Characterization and Analysis of Intra-body Communication Channel," *2009 IEEE Antennas and Propagation Society International Symposium and Usnc/Ursi National Radio Science Meeting, Vols 1-6*, pp. 1820-1823, 2009. [Online]. Available: Go to ISI://WOS:000277085400457.

[22] Z. Lucev et al, "A Capacitive Intrabody Communication Channel from 100 kHz to 100 MHz," *IEEE T Instrum Meas*, vol. 61, no. 12, pp. 3280-3289, Dec 2012, doi: 10.1109/Tim.2012.2205491.

[23] J. Bae et al, "The Signal Transmission Mechanism on the Surface of Human Body for Body Channel Communication," *IEEE T Microw Theory*, vol. 60, no. 3, pp. 582-593, Mar 2012, doi: 10.1109/Tmtt.2011.2178857.

[24] M. A. Callejon et al, "A Comprehensive Study into Intrabody Communication Measurements," *IEEE T Instrum Meas*, vol. 62, no. 9, pp. 2446-2455, Sep 2013, doi: 10.1109/Tim.2013.2258766.

[25] N. Zedong et al, "An Investigation on Dynamic Human Body Communication Channel Characteristics at 45 MHz in Different Surrounding Environments," *IEEE Antennas and Wireless Propagation Letters*, vol. 13, pp. 309-312, 2014, doi: 10.1109/Lawp.2014.2305734.

[26] S. Maity et al, "Characterization of Human Body Forward Path Loss and Variability Effects in Voltage-Mode HBC," *IEEE Microw Wirel Co*, vol. 28, no. 3, pp. 266-268, Mar 2018, doi: 10.1109/Lmwc.2018.2800529.

[27] J. Park et al, "Channel Modeling of Miniaturized Battery-Powered Capacitive Human Body Communication Systems," *IEEE T Bio-Med Eng*, vol. 64, no. 2, pp. 452-462, Feb 2017, doi: 10.1109/Tbme.2016.2560881.

[28] A. Datta et al, "Advanced Biophysical Model to Capture Channel Variability for EQS Capacitive HBC," *arXiv preprint arXiv:2010.15339*, 2020.

[29] D. Das et al, "Enabling Covert Body Area Network using Electro-Quasistatic Human Body Communication," *Sci Rep-Uk*, vol. 9, Mar 11 2019, doi: ARTN 4160 10.1038/s41598-018-38303-x.

[30] S. Lee et al, "A Low-Energy Inductive Coupling Transceiver With Cm-Range 50-Mbps Data Communication in Mobile Device Applications," *IEEE J Solid-St Circ*, vol. 45, no. 11, pp. 2366-2374, Nov 2010, doi: 10.1109/Jssc.2010.2065850.

[31] F. Inanlou and M. Ghovanloo, "Wideband Near-Field Data Transmission Using Pulse Harmonic Modulation," *IEEE T Circuits-I*, vol. 58, no. 1, pp. 186-195, Jan 2011, doi: 10.1109/Tcsi.2010.2055351.

[32] H. J. Kim et al, "Near-Field Magnetic Induction MIMO Communication Using Heterogeneous Multipole Loop Antenna Array for Higher Data Rate Transmission," *IEEE Transactions on Antennas and Propagation*, vol. 64, no. 5, pp. 1952-1962, May 2016, doi: 10.1109/Tap.2016.2539371.

[33] J. C. Edelmann et al, "Inductive Ear-to-Ear Communication Systems: Coupling Enhancement by Means of Constructional Coil Features," *Proceedings of the 2018 IEEE/Mtt-S International Microwave Biomedical Conference (Imbioc)*, pp. 172-174, 2018. [Online]. Available: Go to ISI://WOS:000502126700135.

[34] J. Park and P. P. Mercier, "17.6 A Sub-40μ W 5Mb/s Magnetic Human Body Communication Transceiver Demonstrating Trans-Body Delivery of High-Fidelity Audio to a Wearable In-Ear Headphone," in *2019 IEEE International Solid-State Circuits Conference-(ISSCC)*, 2019: IEEE, pp. 286-287.

[35] A. D. Yaghjian, "Efficient Computation of Antenna Coupling and Fields within the near-Field Region," *IEEE Transactions on Antennas and Propagation*, vol. 30, no. 1, pp. 113-128, 1982, doi: Doi 10.1109/Tap.1982.1142752.

[36] A. H. Akgiray and Y. Rahmat-Samii, "Mutual coupling between two arbitrarily oriented and positioned antennas in near-and far-field regions," in *2010 URSI International Symposium on Electromagnetic Theory*, 2010: IEEE, pp. 780-783.

[37] Y. S. Chen et al, "Analysis of Antenna Coupling in Near-Field Communication Systems," *IEEE Transactions on Antennas and Propagation*, vol. 58, no. 10, pp. 3327-3335, Oct 2010, doi: 10.1109/Tap.2010.2055782.

[38] M. Manteghi et al, "On the Study of the Near-Fields of Electric and Magnetic Small Antennas in Lossy Media," *IEEE Transactions on Antennas and Propagation*, vol. 62, no. 12, pp. 6491-6495, Dec 2014, doi: 10.1109/Tap.2014.2359499.

[39] H. Z. Guo, "Performance Analysis of Near-Field Magnetic Induction Communication in Extreme Environments," *Prog Electrom Res Le*, vol. 90, pp. 77-83, 2020, doi: 10.2528/Pierl20010702.

[40] H. R. Chuang and W. T. Chen, "Computer simulation of the human-body effects on a circular-loop-wire antenna for radio-pager communications

at 152, 280, and 400 MHz," *IEEE T Veh Technol*, vol. 46, no. 3, pp. 544-559, Aug 1997, doi: Doi 10.1109/25.618179.

[41] G. Koutitas, "Multiple Human Effects in Body Area Networks," *IEEE Antennas and Wireless Propagation Letters*, vol. 9, pp. 938-941, 2010, doi: 10.1109/Lawp.2010.2082485.

[42] S. Gabriel et al, "The dielectric properties of biological tissues .2. Measurements in the frequency range 10 Hz to 20 GHz," *Phys Med Biol*, vol. 41, no. 11, pp. 2251-2269, Nov 1996, doi: Doi 10.1088/0031-9155/41/11/002.

[43] A. D. Yaghjian and S. R. Best, "Impedance, bandwidth, and Q of antennas," *IEEE Transactions on Antennas and Propagation*, vol. 53, no. 4, pp. 1298-1324, Apr 2005, doi: 10.1109/Tap.2005.844443.

[44] C. Icheln et al, "Use of balun chokes in small-antenna radiation measurements," *IEEE T Instrum Meas*, vol. 53, no. 2, pp. 498-506, Apr 2004, doi: 10.1109/Tim.2004.823299.

[45] L. J. Xu et al, "Miniaturized Circularly Polarized Loop Antenna for Biomedical Applications," *IEEE Transactions on Antennas and Propagation*, vol. 63, no. 3, pp. 922-930, Mar 2015, doi: 10.1109/Tap.2014.2387420.

[46] G. Varamini et al, "Miniaturization of microstrip loop antenna for wireless applications based on metamaterial metasurface," *Aeu-Int J Electron C*, vol. 83, pp. 32-39, 2018, doi: 10.1016/j.aeue.2017.08.024.